Flexural Behavior of Methyl Methacrylate Modified Unsaturated Polyester Polymer Concrete Beams Reinforced with Glass-Fiber-Reinforced Polymer Sheets

Kyu-Seok Yeon, Yong-Seong Kim, Young-Ik Kim, Yoon-Sang Choi

Department of Regional Infrastructure Engineering, Kangwon National University, Chuncheon 200-701, Korea

Received 24 November 2009; accepted 20 June 2010
DOI 10.1002/app.32990
Published online 28 September 2010 in Wiley Online Library (wileyonlinelibrary.com).

ABSTRACT: This study represents the behavior of flexural test of methyl methacrylate modified unsaturated polyester polymer concrete beam reinforced with glass-fiber-reinforced polymer (GFRP) sheets. The failure mode, load–deflection, ductility index, and separation load predictions according to the GFRP reinforcement thickness were tested and analyzed. The failure mode was found to occur at the bonded surface of the specimen with 10 layers of GFRP reinforcement. For the load–deflection curve, as the reinforcement thickness of the GFRP sheet increased, the crack load and ultimate load greatly increased, and the ductility index was found to be the highest for the beam with the thickness of the GFRP sheet at 10 layers (6 mm) or 13 layers (7.3 mm). The calculated results of separation load were found to match only the experimental results of the specimens where debonding occurred. The reinforcement effect was found to be most excellent in the polymer concrete with 10 layers of GFRP sheet reinforcement. The appropriate reinforcement ratio for the GFRP concrete beam suggested by this study was a fiber-reinforced-plastic cross-sectional ratio of 0.007–0.008 for a polymer concrete cross-sectional ratio of 1 (width) : 1.5 (depth). J Appl Polym Sci 119: 3297–3304, 2011

Key words: composites; polyesters; structure–property relations

INTRODUCTION

The exterior bonding process of steel plates with epoxy adhesive on concrete structures is a very effective and convenient repair method with a short construction time and structural applicability to not only the tight part but also the part with compressive force and shear force. This method, however, because of steel's weakness of poor corrosion resistance, decreases the bonding power of concrete and the steel sheet and, in turn, deteriorates the performance of the structure.[1,2] Also, because of the heavy weight-to-volume ratio, it requires more labor and equipment for construction. To overcome such shortages of steel, fibers, such as glass fibers, carbon fibers, and aramid fibers, and liquefied polymers, such as polyesters, epoxies, and vinyl esters, are used for the development of glass-fiber-reinforced polymers (GFRPs), carbon-fiber-reinforced polymers, and aramid-fiber-reinforced polymers in sheets of plate formats, which are largely being applied to site constructions.

Correspondence to: Y.-S. Choi (nacys38@kangwon.ac.kr).
Contract grant sponsors: Kangwon National University (KNU), Korea Institute of Construction & Transportation Technology Evaluation and Planning (KICTTEP), National Research Foundation of Korea (NRF).

Journal of Applied Polymer Science, Vol. 119, 3297–3304 (2011)

Experimental research on steel plates and fiber-reinforced plastic (FRP) reinforcement for reinforced concrete (RC) structures has been conducted with various shapes, bonding methods, and so on of structures and various reinforcements, such as GFRPs and carbon-fiber-reinforced polymers in studies by Saadatmanesh and Ehsani,[3] Sharif et al.,[4] Ross et al.,[5] Bahn and Harichandran,[6] and Yang et al.[7] A theoretical study was conducted on the basis of the theoretical model of Roberts,[8] whereas An et al.[9] and Ziraba et al.[10] conducted cross-sectional analyses, and Arduini and Nanni[11,12] divided the thickness of FRP into very small areas and determined the stress for that small area. Also, Malek et al.[13] suggested a general solution by considering the axial strain and flexural strain, and Smith and Teng[14] suggested a general solution by considering the axial strain, flexural strain, and shear strain. In addition, Chaallal et al.[15] suggested guidelines for the shear and flexure of beams strengthened with externally bonded FRP according to the Canadian Concrete Standard, and Chen and Qiao[16] suggested a prediction formula of ductility and ultimate load through interfacial stress analysis. Such studies on structural testing and analysis with regard to FRP exterior bonding methods began in the late 1980s and have been applied to structures in various ways since.

Generally, beams strengthened with externally bonded FRPs usually bring debonding. The failure

mode of debonding exhibits ductile failure at first and then brittle failure so that its use requires careful consideration. Also, this method has only been studied with regard to RC structures, and it is difficult to find research results for polymer concretes.

Therefore, in this study, the flexural behavior was tested for polymer concrete beams reinforced with GFRPs attached to the exterior. That is, by investigating the flexural behavior and reinforcement effects, such as the failure mode, load–deflection relationship, ductility index, moment characteristics, prediction of stress, and separation load within the bonding surface, we intended to create an elementary resource for structural design, such as the calculation of the appropriate reinforcement thickness of GFRP sheets according to the cross-sectional thickness of the polymer concrete beams.

EXPERIMENTAL

Materials

Polymer concrete

Polymer concrete uses ortho-type unsaturated polyester (UP) resin with added cobalt-type hardening accelerator as the major binder. Also, for workability improvement and resin usage reduction, methyl methacrylate (MMA) monomer was mixed at a 30% ratio compared to the weight of the major binder and used.

Table I shows the characteristics of the UP resin and MMA monomer used. Also, for reduced contraction during hardening, a contraction reducer with thermoplastic polystyrene dissolved in styrene monomer was used; its characteristics are shown in Table II.

Silica, sand-dried for 24 h at 110 ± 5°C to achieve a water content below 0.1%, was used for the aggregate, whose physical characteristics are shown in Table III. For the filler, because of the workability of polymer concrete, heavy calcium carbonate with a fineness of 2500–3000 cm^2/g and a particle size of 1–30 μm was used, and its physical and chemical properties are shown in Table IV.

The mixing proportion of the polymer concrete is shown in Table V. As shown in Table V, UP resin as the binder took up 9% of the whole weight, and the MMA monomer was 30% of the binders. Also, with consideration of the strength and workability, the ratio of the sealant to the binders was set as 2 : 1, and the ratio of the fine aggregate to the coarse aggregate was set as 1.5 : 1.

TABLE I
Properties of the UP Resin and MMA Monomer

	Density at 20°C (g/cm^3)	Viscosity at 20°C (mPa·s)	Acid value	Styrene content (%)
UP resin	1.13	300	20.0	40.0
	Density at 20°C (g/cm^3)	Viscosity at 20°C (mPa·s)	Molecular weight	Appearance
MMA monomer	0.942	0.56	100	Transparent

TABLE II
Properties of the Shrinkage-Reducing Agent

Density at 20°C (g/cm^3)	Viscosity at 20°C (mPa·s)	Nonvolatile matter (%)	Appearance
1.11	3100–4100	34–38	Transparent

GFRP sheets

In this study, E-glass fiber, widely in use for reinforcement, was used. To manufacture GFRP sheets for tensile-part reinforcement of the beam, roving cloth with a thickness of 0.6 mm was used, and its characteristics are shown in Table VI.

Preparation of the specimens

For the beam production material, polymer concrete with a compressive strength of 90 MPa, a flexural strength of 17 MPa, a splitting tensile strength of 12 MPa, a modulus of elasticity of 24.0 GPa, and a Poisson's ratio of 0.22 was used, and for the GFRP reinforcement material, GFRP with a tensile strength of 260–290 MPa and a modulus of elasticity of 10.2 GPa was used. The glass fiber for GFRP was placed one by one with a hand lay-up method, which was easy to process, and polymer concrete was placed before the deposited resin hardened for the maximum bonding performance. The specimen was cured at 23 ± 2°C for a week before the deflection test was conducted. The specification of the specimen used in this study is shown in Table VII and Figure 1, and it had span of 800 mm and a cross section of 100 mm (width) × 150 mm (height).

The deflection test was conducted with a universal testing machine (Instron Co., Norwood) with a capacity of 250 kN. As for the testing method, in compliance with ASTM C78-94 (Standard Test Method for Flexural Strength of Concrete; Using Simple Beam with Third-Point Loading), four-point loading was applied with the loading control method (1.54 kN/

TABLE III
Physical Properties of the Aggregates

Size (mm)	Density at 20°C (g/cm^3)	Moisture content (%)	Organic impurities
5.0–13.0	2.78	<0.1	None
0.8–5.0	2.62	<0.1	None
0.0–0.8	2.45	<0.1	None

TABLE IV
Physical and Chemical Properties of Heavy Calcium Carbonate

	Density (g/cc)	Absorption (cc/g)	Water content (%)	pH	Mean grain size (μm)	Retained percentage of the 325-mesh sieve
Physical properties	0.75	0.20	<0.1	8.8	13	0.03
	CaO	Al_2O_3	Fe_2O_3	SiO_2	MgO	Ignition loss
Chemical components	53.7	0.25	0.09	2.23	0.66	42.4

TABLE V
Mixing Proportions of the Polymer Concrete

Binder content (mass %)	Binder formation					Aggregate ratio	
	UP	MMA	Methyl ethyl ketone peroxide	N,N-dimethyl aniline	Filler/binder	Fine	Coarse
9.0	70	30	0.75	0.50	2.0/1.0	1.5	1.0

min) until final failure, and simple supports were used for points.

RESULTS AND DISCUSSION

Failure mode

In general, the final failure mode of the exterior bonding method has the bonding failure occurring from the interface between the RC and the reinforcement material as the major cause,[17] and the bonding failure is divided into the end-region bonding failure, where the failure begins from the end-region of the reinforcement material, and the middle-region bonding failure, where the failure begins from the crack of the RC.[18,19]

Figure 2 shows the final failure mode of the polymer concrete according to the thickness of the GFRP sheet reinforcement. In such results, the case with no GFRP sheet reinforcement (GFRP-0) exhibited simultaneous failure with the initial crack occurring at the middle point of the beam. Also, for the GFRP-2 (1.2 mm), GFRP-5 (3 mm), and GFRP-8 (4.8 mm) specimens, the final failure occurred at the GFRP, and the GFRP reinforcement was found to suppress crack advancement to a degree after the initial crack occurrence. For the GFRP-10 (6 mm), GFRP-13 (7.8 mm), GFRP-15 (9 mm), and GFRP-20 (12 mm) specimens, failure mode due to the debonding of GFRP and polymer concrete was observed. Particularly for the cases with reinforcements over 10 layers of GFRP (6.0 mm), the final failure mode of debonding of GFRP and polymer concrete occurred quickly and suddenly, so this an important point to consider in application to actual structures.

TABLE VI
Physical Properties of the Roving Cloth

Count (yarns/in.)					
Wrap	Fill	Weave	Weight (g/m^3)	Width (mm)	Thickness (mm)
6.3	6.3	Plain	580	1000	0.6

Load–deflection

The load–deflection curve of general RC beams reinforced with externally bonded FRP was divided into three sections: the crack transfer section, yield transfer section, and postyield section.[5,20,21] In this study, however, as there was no tensile-part rebar reinforcement, an exact yield section did not appear; therefore, it was represented with two sections of precrack (linear) and postcrack (nonlinear) according to the initial crack of the polymer concrete.

Figure 3 shows the load–deflection relationship according to GFRP reinforcement thickness. Here, in the case of without GFRP sheet reinforcement (GFRP-0), no additional increase in loading weight or deflection occurred because of brittle failure after initial crack occurrence, and it exhibited ductile behavior until failure. GFRP-2 (1.2 mm), almost

TABLE VII
Details of the Beam Specimen

Series	Width (mm)	Depth (mm)	Length (mm)	GFRP sheet	
				Layer	Thickness (mm)
GFRP-0	100	150	1000	0	0
GFRP-2				2	1.2
GFRP-5				5	3.0
GFRP-8				8	4.8
GFRP-10				10	6.0
GFRP-13				13	7.8
GFRP-15				15	9.0
GFRP-20				20	12.0

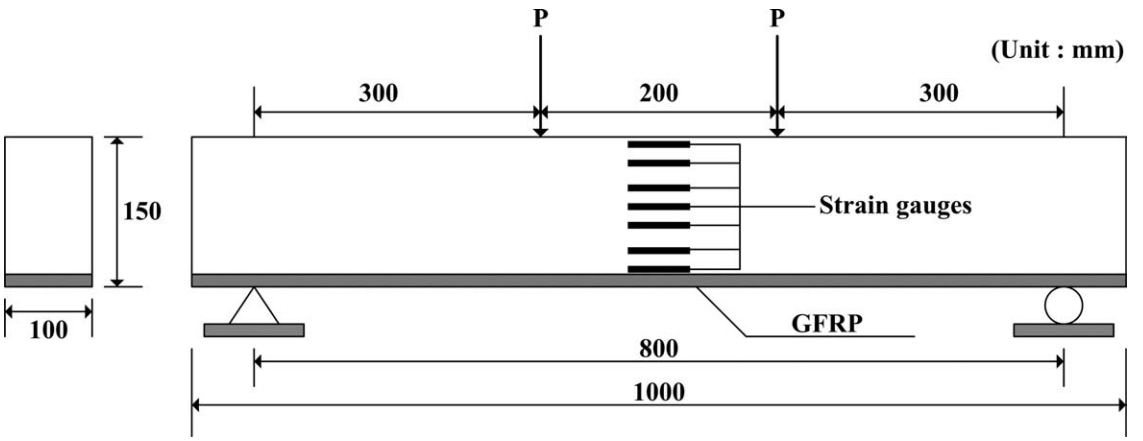

Figure 1 Test scheme for the beam specimen.

identical to GFRP-0, exhibited failure after the initial crack occurrence. This was interpreted as follows: when the thickness of the reinforcement material was too small, it did not affect the failure behavior of the polymer concrete very much. In the case of GFRP-5 (3.0 mm) and GFRP-8 (4.8 mm), unlike GFRP-0 and GFRP-2 (1.2 mm), the deflection after the initial crack occurrence showed a tendency to increase continually until failure, but the increase in the ultimate load was very small. GFRP-10 (6.0 mm) showed almost identical tendencies as GFRP-8 in crack load and deflection in crack load, but the ultimate load and the deflection in ultimate load were increased by about 20 kN and 5 mm, respectively. These results show that compared to GFRP-8, GFRP-10 exhibited ductile behavior after the crack load. On the other hand, the crack load and the deflection in crack load of GFRP-13 (7.8 mm) was found to be similar to GFRP-10, but the ultimate load was found to be increased greatly. Next, for GFRP-15 (9.0 mm) and GFRP-20 (12.0 mm), the crack load and ultimate load were found to be increased greatly, but the deflection increase after crack load was almost identical to that of GFRP-10. For the GFRP-10, GFRP-13, GFRP-15, and GFRP-20 specimens, debonding occurred so that when the cracking occurred rapidly, the failure occurred with an increase in load without much increase in deflection. From such analysis results of the load–deflection curve, we concluded that in design, the thickness of the GFRP sheet reinforcement must be decided with consideration of the ultimate load and ductile behavior characteristics.

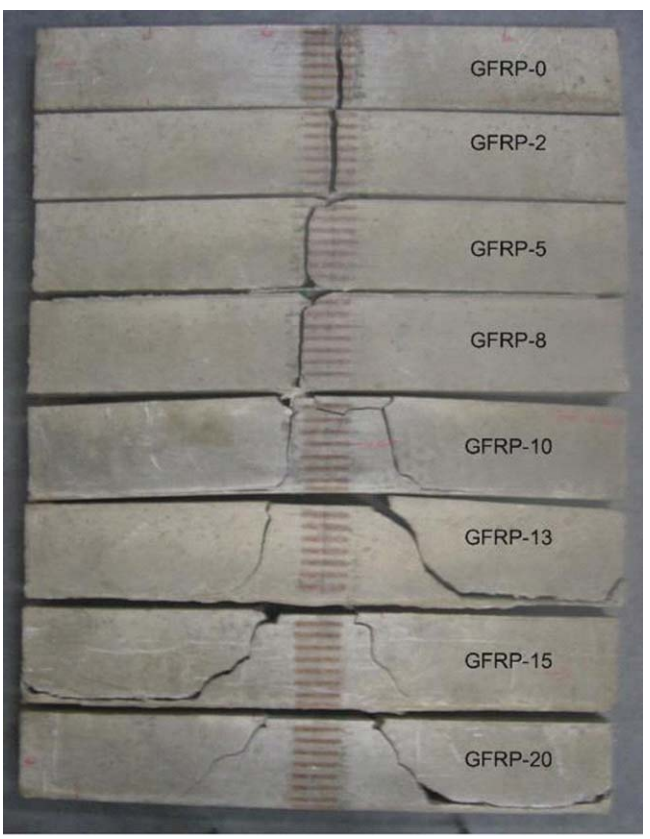

Figure 2 Failure mode of the specimens. [Color figure can be viewed in the online issue, which is available at wileyonlinelibrary.com.]

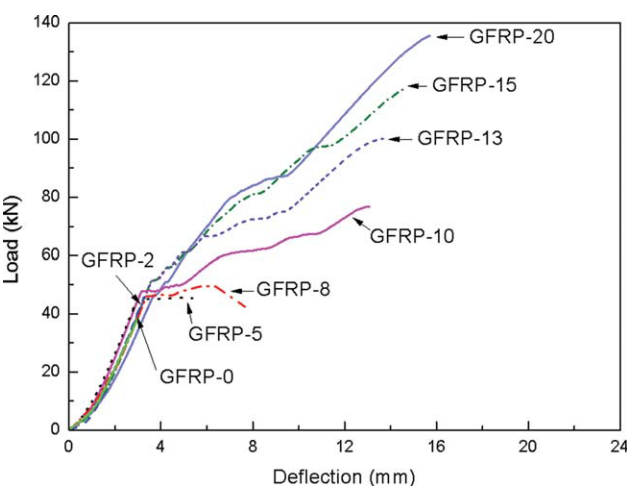

Figure 3 Load–deflection curves. [Color figure can be viewed in the online issue, which is available at wileyonlinelibrary.com.]

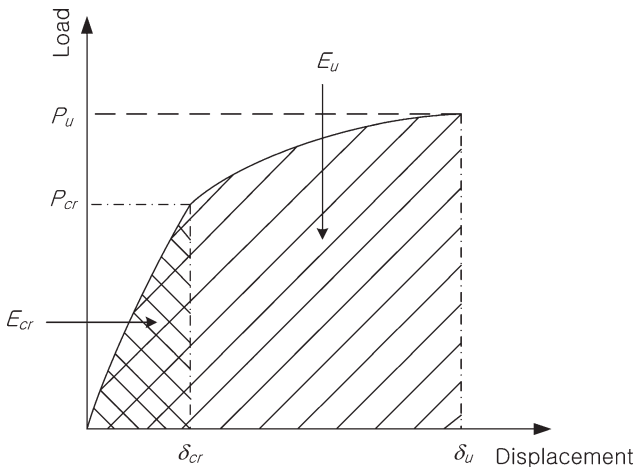

Figure 4 Idealized load–displacement curve. P_{cr} = cracking load; P_u = ultimate load; δ_{cr} = midspan deflection at cracking load; δ_u = midspan deflection at ultimate load.

Ductility index

In this study, because of the absence of tensile-part rebar reinforcement, the exact yield section could not be represented, so the displacement ductility index and the strain energy ductility index at the crack load and the ultimate load were compared.

Displacement ductility index

As shown in Figure 4,[22,23] the results of the calculation of the displacement ductility index with displacement at the crack load and the ultimate load are shown in Table VIII:

$$\mu_\Delta = \frac{\Delta_u}{\Delta_{cr}} \tag{1}$$

where μ_Δ is the displacement ductility index, Δ_u is the midspan deflection at ultimate load, and Δ_{cr} in the midspan deflection at cracking load.

For GFRP-0, the ductility index was 1.0 as the beam failed at yield load; this showed that the yield load and the ultimate load were the same, and in turn, the displacements were the same. For GFRP-2, the GFRP sheets were reinforced, but the effects were insignificant. The ductility indices of GFRP-10 and GFRP-13, where deflection began to increase greatly, were found to be very great compared to those of other specimens. On the other hand, GFRP-15 and GFRP-20 exhibited lower ductility indices compared to GFRP-10 and GFRP-13 with less GFRP sheet reinforcement. These results reflect the fact that GFRP sheet reinforcement over a certain thickness did not contribute to the improvement of the beam's flexural strength and deformability, and also, the brittle failure mode combining bonding failure and deflection failure was exhibited.

Strain energy ductility index

We obtained the strain energy by calculating the area under the load–displacement curve of Figure 4.[22,23] In this study, the area of the load–deflection curve for the deflection at the crack load and the ultimate load was integrated to obtain the strain energy. Also, the strain energy ductility index was calculated with eq. (2):

$$\mu_E = \frac{E_u}{E_{cr}} \tag{2}$$

where μ_E is the strain energy ductility index, E_u is the area under the load–deflection diagram at ultimate load (total energy), and E_{cr} is the area under the load–deflection diagram at cracking load.

Table IX shows the strain energy and strain energy ductility index. Strain energy ductility index was the highest for GFRP-15 at 10.14 and for GFRP-13 and GFRP-10 at 8.97 and 8.67, respectively. Overall, it exhibited a tendency similar to the displacement ductility index, but the fact the GFRP-15 was found to have especially high results was due to the fact that the load and deflection dramatically increased because of crack occurrence compared to GFRP-13.

TABLE VIII
Displacement Ductility Index

Series	Cracking load (kN)	Cracking deflection (mm)	Ultimate load (kN)	Ultimate deflection (mm)	Ductility index (displacement)[a]
GFRP-0	38	3.0	38	3.0	1.00
GFRP-2	45	3.2	46	3.3	1.03
GFRP-5	46	3.5	54	6.9	3.40
GFRP-8	48	3.7	59	8.4	2.27
GFRP-10	50	3.8	77	13.1	3.44
GFRP-13	52	4.0	100	13.7	3.43
GFRP-15	54	8.5	117	14.7	1.73
GFRP-20	60	9.2	135	15.6	1.70

[a] Ultimate deflection/cracking deflection.

TABLE IX
Strain Energy Ductility Index

Series	Cracking load (kN)	Cracking strain energy (J)	Ultimate load (kN)	Ultimate strain energy (J)	Ductility index (strain energy)[a]
GFRP-0	38	46.75	38	46.75	1
GFRP-2	45	49.57	46	56.74	1.15
GFRP-5	46	56.43	54	165.33	2.93
GFRP-8	48	64.32	59	266.62	4.15
GFRP-10	50	77.45	77	671.57	8.67
GFRP-13	52	93.53	100	838.75	8.97
GFRP-15	54	100.11	117	1015.46	10.14
GFRP-20	60	141.42	135	1189.78	8.41

[a] Ultimate strain energy/cracking strain energy.

TABLE X
Moment and Ultimate Moment Strength

Series	Cracking moment (kN·cm)	Ultimate moment (kN·cm)	Cracking moment/ultimate moment	Ultimate moment strength: Ultimate moment/bd^2 (N·mm/mm^3)
GFRP-0	570	570	1	2.53
GFRP-2	675	690	0.98	3.07
GFRP-5	690	810	0.85	3.60
GFRP-8	720	885	0.81	3.93
GFRP-10	750	1155	0.65	5.13
GFRP-13	780	1500	0.52	6.67
GFRP-15	810	1755	0.46	7.80
GFRP-20	900	2025	0.44	9.00

b = width of the beam; d = depth of the beam.

Ultimate moment strength

Table X shows the crack moment, ultimate moment, and ultimate moment strength of GFRP-reinforced polymer concrete. The crack moment, ultimate moment, and ultimate moment strength all increased as the GFRP thickness increased. This indicated that GFRP exhibited tensile reinforcement effects as a reinforcement material by generating a sufficient resistance moment. In particular, as shown in Figure 5, GFRP-10 and GFRP-13 exhibited about a 30% increase; this rate of increase was greater than those of GFRP-15 and GFRP-20 with more reinforcement.

Analysis of interfacial stress

Between the polymer concrete and GFRP, shear stress and normal stress applied.[24] The GFRP-reinforced polymer concrete used in this study was of the precast type so that the following equations, suggested by Roberts,[8] were used for stress analysis:

$$\tau_{max} = \left[F_0 + \left(\frac{K_s}{E_{frp} b_{frp} d_{frp}}\right)^{\frac{1}{2}} M_0\right] \frac{b_{frp} d_{frp}}{I b_a} (h_{frp} - h) \quad (3)$$

$$\sigma_{max} = \tau_{max} d_{frp} \left(\frac{K_n}{4 E_{frp} I_{frp}}\right)^{\frac{1}{4}} \quad (4)$$

where σ_{max} is the maximum normal stress, τ_{max} is the maximum shear stress, $K_s = G_a(b_a/d_a)$ is the

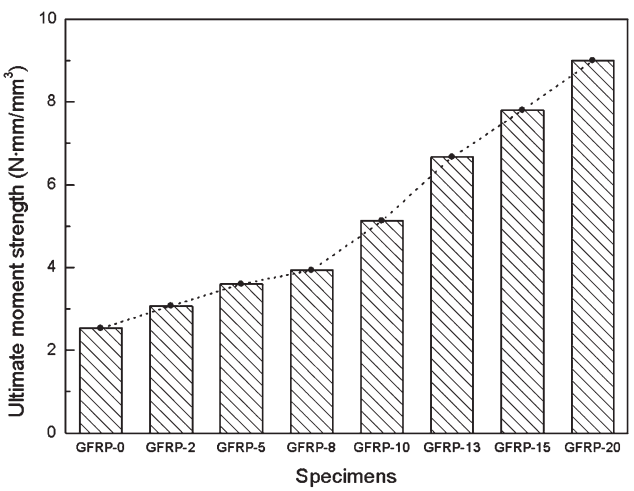

Figure 5 Comparison of the ultimate moment strength.

TABLE XI
Results of the Analysis of Interfacial Stress

Series	τ_{max} (MPa)	σ_{max} (MPa)
GFRP-0	Not applicable	Not applicable
GFRP-2	1.36	0.73
GFRP-5	3.59	2.42
GFRP-8	7.33	5.55
GFRP-10	9.02	7.23
GFRP-13	12.84	10.99
GFRP-15	14.99	13.29
GFRP-20	18.80	17.91

shear stiffness per unit length, $K_n = E_a(b_a/d_a)$ is the normal stiffness per unit length, F_0 is the global shear force in the beam, E_{frp} is the Young's modulus of FRP, b_{frp} is the width of FRP, d_{frp} is the depth of FRP, M_0 is the global bending moment, I is the geometrical moment of inertia of the full composite, b_a is the width of the adhesive layer, h_{frp} is the effective depth of FRP, h is the depth of neutral axis, I_{frp} is the geometrical moment of inertia, G_a is the shear modulus of the adhesive, d_a is the depth of the adhesive layer, and E_a is the Young's modulus of the adhesive.

These formulas are intended for the calculation of separation load, and the interfacial stress at ultimate load was calculated as shown in Table XI. GFRP-2 and GFRP-5 showed results similar to the test results of the RC concrete with a GFRP plate (thickness = 4 mm),[14] and for GFRP-8 and greater, the stress was found to be very large. As the thickness of the GFRP sheet reinforcement increased, the interfacial stress also increased, and Figure 6 shows the interfacial stress according to the thickness of the GFRP sheet per specimen.

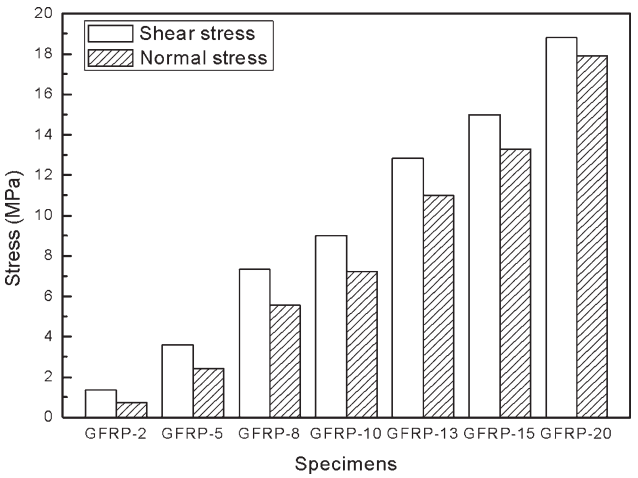

Figure 6 Effect of the GFRP sheet thickness on the interfacial stresses.

Prediction of the separation load

In a FRP–RC beam, debonding generally begins with the initial crack occurring at the polymer concrete and advances rapidly to failure without much increase in deflection, as shown in Figure 7, so it is very important to predict the separation load.

The separation load (P), in consideration of interfacial stress, was obtained through the following equation suggested by Banh and Harichandran:[6]

$$P = \frac{2\tau_0}{\left[1 + \left(\frac{K_s}{E_{frp} b_{frp} t_{frp}}\right)^{\frac{1}{2}} \left(1 + \frac{h_{pc} t_{frp}}{2}\right)\right] \frac{b_{frp} t_{frp}}{I b_a} (h_{frp} - h)} \quad (5)$$

where τ_0 is the maximum shear stress at the interface, b_{frp} is the width of FRP, h_{pc} is the height of the polymer concrete beam, h is the depth of neutral axis, and t_{frp} is the thickness of FRP.

τ_0 is the interfacial stress obtained from eq. (3), which was substituted in eq. (5) to calculate the separation load. Table XII shows the comparison of the load value measured through the experiment and the calculated value. As the result, for the beams where the failure occurred at the bonding surface of the GFRP sheet and polymer concrete (GFRP-10, GFRP-13, GFRP-15, and GFRP-20), the experimental value and the calculated value were found to nearly match, but for the beams that exhibited direct tensile destruction of FRP (GFRP-2, GFRP-5, and GFRP-8), those two values showed a great difference. This indicated that when the beam was under deflection load, the tensile strength of FRP was weaker than the load working on the bonding surface so that FRP failed first.

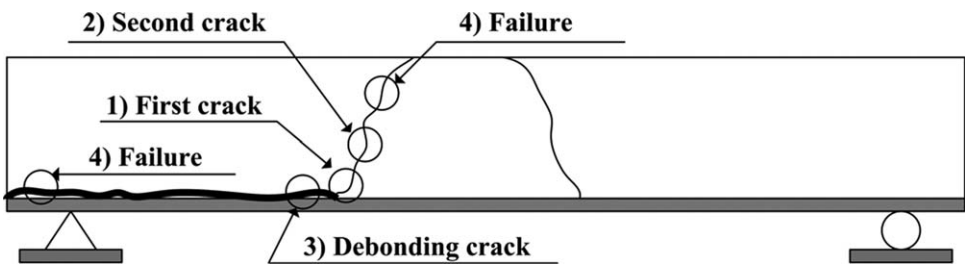

Figure 7 Idealized crack pattern.

TABLE XII
Comparison of the Measured and Calculated Failure Loads

Series	Measured failure load (kN)	Calculated failure load (kN)	Calculated failure load/ measured failure load	Failure mode
GFRP-2	46	116.41	2.53	FRP rupture
GFRP-5	54	90.63	1.68	FRP rupture
GFRP-8	59	80.57	1.37	FRP rupture
GFRP-10	77	95.41	1.24	FRP debonding
GFRP-13	100	110.56	1.11	FRP debonding
GFRP-15	117	121.55	1.04	FRP debonding
GFRP-20	135	123.68	0.92	FRP debonding

CONCLUSIONS

In this study, we experimentally investigated the behavior of the deflection of an MMA-modified UP polymer concrete beam reinforced with GFRP sheets, and the results are as follows.

The failure mode was found to be deflection failure without reinforcement; FRP tensile failure for reinforcement with 2 layers (1.2 mm), 5 layers (3.0 mm), and 8 layers (4.8 mm) of GFRP; and failure at the bonding interface of FRP and polymer concrete for 10 layers (6.0 mm), 13 layers (7.8 mm), 15 layers (9.0 mm), and 20 layers (12.0 mm) of GFRP. In the load–deflection curve, 2 layers of GFRP exhibited failure after initial crack occurrence just like without GFRP; this indicated that if the reinforcement layer was too thick, the elastic behavior of the polymer concrete was fine, but there was little influence on the failure mechanism. The ductility index was found to be the most excellent for the reinforcement with 10 and 13 layers of GFRP, and the strain energy ductility index was found to be the most excellent for reinforcement with 13 and 15 layers of GFRP. This indicated that GFRP sheet reinforcement over a certain thickness did not contribute much to the improvement of the flexural strength or deflection control. The ultimate moment strength showed a tendency to increase as the thickness of the GFRP sheet increased, but because of the failure mode or ductility index, overreinforcement of more than 15 layers was found to be ineffective. With the separation load calculated with the interfacial stress at the bonding surface considered, only the beams that failed at the bonding surface showed a calculated value that matched the experimental value. The reinforcement effect was found to be most excellent in the polymer concrete with 10 layers of GFRP sheet reinforcement. Combining the above results, we found that the appropriate reinforcement ratio for the GFRP-reinforced polymer concrete beam suggested by this study was a GFRP cross-sectional ratio of 0.007–0.008 for a polymer concrete cross-sectional ratio of 1 (width) : 1.5 (depth).

References

1. ACI Committee 440. State of-the-Art Report on Fiber Reinforced Plastic (FRP) Reinforcement for Concrete Structures; American Concrete Institute: Farmington Hills, MI, 1996.
2. Hosny, A.; Shaheen, H.; Abdelrahman, A.; Elafandy T. Cem Concr Compos 2006, 28, 906.
3. Saadatmanesh, H.; Ehsani, M. R. J. Struct Eng 1991, 117, 3417.
4. Sharif, A.; Al-Sulaimani, G. J.; Basunbul, I. A.; Baluch, M. H.; Ghaleb, B. N. ACI Struct J 1994, 91, 160.
5. Ross, C. A.; Jerome, D. M.; Tedesco, J. W.; Hughes, M. L. ACI Struct J 1999, 96, 212.
6. Bahn, B. Y.; Harichandran, R. S. J. Compos Constr 2008, 12, 387.
7. Yang, D. S.; Park, S. K.; Neale, K. W. Compos Struct 2008, 88, 497.
8. Roberts, T. M. Struct Eng (London) 1989, 67, 228.
9. An, W.; Saadatmanesh, H.; Ehsani, M. R. J. Struct Eng 1991, 117, 3434.
10. Ziraba, Y. N.; Baluch, M. H.; Basunbul, I. A.; Sharif, A. M.; Azad, A. L.; Al-Sulaimani, G. J. ACI Struct J 1994, 91, 639.
11. Arduini, M.; Nanni, A. ACI Struct J 1997, 94, 363.
12. Arduini, M.; Nanni, A. ACI Struct J 1997, 94, 493.
13. Malek, A. M.; Saadatmanesh, H.; Ehsani, M. R. ACI Struct J 1998, 95, 142.
14. Smith, S. T.; Teng, J. G. Eng Struct 2001, 23, 857.
15. Chaallal, O.; Nollet, M. J.; Perraton, D. Can J Civ Eng 1998, 25, 692.
16. Chen, F.; Qiao, P. Int J Solids Struct 2009, 46, 2618.
17. Jianwu, P.; Shuangyin, C. In Proceedings of the International Symposium in Bond Behaviors of FRP in Structures Hong Kong; International Institute for FRP in Construction: Winnipeg, Manitoba, Canada, 2005; p 291.
18. Achintha, P. M. M.; Burgoyne, C. J. J. Compos Constr 2008, 12, 396.
19. Achintha, P. M. M.; Burgoyne, C. J. ACI Struct J 2009, 106, 20.
20. El-Mihilmy, M. T.; Tedesco, J. W. ACI Struct J 2000, 97, 679.
21. El-Mihilmy, M. T.; Tedesco, J. W. J. Struct Eng 2000, 126, 684.
22. Grace, N. F.; Soliman, A. K.; Abdel-Sayed, G.; Saleh, K. R. J. Compos Constr 1998, 2, 186.
23. Jo, B. W.; Tae, G. H.; Kwon, B. Y. J. Reinforc Plast Compos 2004, 23, 843.
24. Li, L.; Guo, Y.; Liu, F. Constr Build Mater 2008, 22, 315.